ELSEVIER

International Journal of Mass Spectrometry 207 (2001) 223–239

International Journal of Mass Spectrometry

Time-of-flight mass spectrometry study of the fragmentation of valence shell ionised nitrobenzene

L. Cooper[a], L.G. Shpinkova[b], E.E. Rennie[c], D.M.P. Holland[d,*], D.A. Shaw[d]

[a] Department of Chemistry, Heriot-Watt University, Riccarton, Edinburgh, EH14 4AS, UK
[b] Department of Nuclear Spectroscopy Methods, Institute of Nuclear Physics, Moscow State University, Moscow 119899, Russian Federation
[c] Fritz-Haber Institute, Department of Surface Physics, Faradayweg 4-6, D-14195 Berlin, Germany
[d] Daresbury Laboratory, Daresbury, Warrington, Cheshire, WA4 4AD, UK

Received 2 October 2000; accepted 29 January 2001

Abstract

A time-of-flight mass spectrometry study has been carried out to investigate the fragmentation processes occurring in nitrobenzene as a result of valence shell photoionisation. Synchrotron radiation has been used to record spectra in the photon energy range 11–31 eV, and appearance energies have been determined for 18 fragment ions. These have enabled, previously unknown, heats of formation to be estimated for $C_5H_2^+$ and $C_6H_3^+$. The fragment ion appearance energies have been compared to similar data for benzene and toluene in order to highlight the influence of the substituent on the fragmentation patterns. The time-of-flight spectra show that the peak associated with the NO^+ fragment changes shape as a function of excitation energy, and at high photon energy the peak consists of two components, one of which is narrow and the other broad. The latter component is due to fragments possessing substantial initial kinetic energy. In contrast, the peak associated with the NO_2^+ fragment always appears broad. This behaviour is discussed in relation to the initial formation of a doubly charged ion and a subsequent coulomb repulsion. In a separate experiment the absolute photoabsorption cross section of nitrobenzene has been measured between the ionisation threshold and 35 eV using a double ion chamber. Some of the broad features have been attributed, tentatively, to valence shell excitations into π^* orbitals. (Int J Mass Spectrom 207 (2001) 223–239) © 2001 Elsevier Science B.V.

Keywords: Photoionisation; appearance energy; Synchrotron radiation

1. Introduction

The dissociation dynamics of the nitrobenzene molecular ion have been the subject of numerous experimental and theoretical studies, and the principal fragmentation processes are now fairly well established. The experimental work has employed a variety of techniques, such as conventional mass spectrometry [1–15], threshold-photoelectron-photoion-coincidence (TPEPICO) spectroscopy [16–18], and infrared multiphoton absorption [19,20]. The results from several of these studies have been interpreted using predictions based on statistical models.

Although the main fragmentation processes are well understood, much less attention has been focused on the weaker channels and on those whose thresholds occur at high energy. In the present work, all the

* Corresponding author. E-mail: d.m.p.holland@dl.ac.uk

PII S1387-3806(01)00374-8

dissociation processes occurring up to 31 eV have been investigated by means of time-of-flight (TOF) mass spectrometry. Particular attention has been paid to the manner in which the NO_2 substituent influences the thermodynamics of the fragmentation phenomena observed following outer valence shell photoionisation. In earlier mass spectrometry studies we have investigated the basic π aromatic electron system of benzene [21] and have studied the effect of replacing C_2H_2 by a heteroatom, e.g. in furan [22], pyrrole [23], and thiophene [24], or of attaching monosubstituents of varying chemical nature, eg in toluene [25]. The present data for nitrobenzene will be compared to the results from these related studies, and discussed in terms of the electron donating or withdrawing character of the substituent.

Previous work has established that the principal fragmentation processes observed in nitrobenzene after outer valence shell photoionisation are

$$C_6H_5NO_2^+ \rightarrow C_6H_5O^+ + NO \quad (A)$$

$$C_6H_5NO_2^+ \rightarrow C_6H_5^+ + NO_2 \quad (B)$$

$$C_6H_5NO_2^+ \rightarrow C_5H_5^+ + CO + NO \quad (C)$$

$$C_6H_5NO_2^+ \rightarrow C_4H_3^+ + (NO + C_2H_2O)/(NO_2 + C_2H_2) \quad (D)$$

$$C_6H_5NO_2^+ \rightarrow C_3H_3^+ + NO + CO + C_2H_2 \quad (E)$$

$$C_6H_5NO_2^+ \rightarrow NO^+ + C_6H_5O \quad (F)$$

Allam et al. [12,13] studied both normal and deuterated nitrobenzene, using electron impact, and determined the relative intensities for the most intense fragment ions—$C_6H_5O^+$, $C_6H_5^+$, $C_4H_3^+$, and NO^+—arising through processes (A), (B), (D), and (F), respectively. Appearance energies for $C_6H_5^+$, $C_6D_5^+$, $C_4H_3^+$, and $C_4D_3^+$ were also measured. Similar information was obtained by Matyuk et al. [7] by using photon excitation. The competition between direct bond cleavage, losing NO_2 [process (B)] and rearrangement, leading to the loss of NO [process (A)] has been the focus of several electron impact [1–4,9,10] and chemical ionisation [5,6] mass spectrometry studies.

Panczel and Baer [16] used the TPEPICO technique to derive the first nitrobenzene breakdown curves for the molecular ion and for the fragments formed through processes (A)–(F), over the photon energy range 10–13.3 eV. Decay rate constants and kinetic energy releases were also determined for selected fragments. Similar information was obtained by Nishimura et al. [18], who used the same experimental technique but over an extended (10–18 eV) range. The breakdown curves recorded in these two studies were quite similar to one another, as expected. Nevertheless, two major differences were observed. The first, and most important, of these differences concerns the $C_4H_3^+$ ion. This ion was observed between 11.4 and 12.65 eV in the breakdown curves presented by Panczel and Baer, and the corresponding neutrals were assigned as $NO+C_2H_2O$. However, Nishimura et al. observed this ion only at energies above 15.66 eV, and assigned the neutrals as $NO_2 + C_2H_2$. The second difference is that although Nishimura et al. found the $C_3H_3^+$ ion to have an appearance energy (AE) of 12.63 eV, Panczel and Baer did not detect this ion at all. Both TPEPICO studies indicated that the $C_6H_5^+$, $C_5H_5^+$, and NO^+ ions were metastable, but Nishimura et al. also reported the $C_6H_5O^+$ and $C_4H_3^+$ ions as being metastable.

The photodissociation of nitrobenzene molecular ions has been investigated after initial formation using electron [8,14] or photon [17] impact. Bunn et al. [17] performed laser induced dissociation studies on energy selected nitrobenzene ions and measured the absolute photodissociation cross section, as well as determining the kinetic energy release distributions for several fragment ions.

The early TPEPICO work [16,18] studied the fragmentation of the nitrobenzene molecular ion on the microsecond timescale. More recently, Hwang et al. [15] have investigated the photodissociation dynamics on the nanosecond timescale using mass analysed ion kinetic energy spectrometry. Their experiment showed that the dissociation channels producing $C_6H_5O^+$, $C_6H_5^+$, and NO^+ occur competitively, and that $C_6H_5O^+$ ions formed with high internal energies dissociate further to produce $C_5H_5^+$. These findings were in agreement with the conclu-

sions of Nishimura et al. [18] but not with those of Panczel and Baer [16].

Moini and Eyler [19] studied the dissociation of nitrobenzene cations using infrared multiphoton excitation and observed three fragment ions, namely $C_6H_5O^+$, $C_5H_5^+$, and NO^+. The $C_6H_5^+$ fragment was not observed even though all four ions have similar appearance energies. This led them to the conclusion that the first three fragments were being produced from high vibrational levels of the ground electronic state of the ion. In contrast, it was postulated that the formation of $C_6H_5^+$ occurred either directly from an excited electronic state or from the ground state via a pathway whose activation energy exceeds that of $C_6H_5O^+$, NO^+, and $C_5H_5^+$ by more than 0.2 eV. However, this latter proposal was not supported by the existing appearance energies. In a recent study performed by Osterheld et al. [20], the production of $C_6H_5^+$ was observed in pulsed infrared multiphoton dissociation, indicating that the formation of this fragment occurs from the ground electronic state. To explain these results, Osterheld et al. proposed that in the formation of some products the nitrobenzene cation dissociates to form an ion-molecule complex and then re-associates to give the phenylnitrite structure.

Nitrobenzene was used as an example molecule by Porter et al. [10] to illustrate the various ways in which a contemporary mass spectrometer can be used to study molecular dissociation phenomena. Amongst the information they obtained was the translational energy released during fragmentation. This was determined from the broadening observed on metastable ion peaks. In particular, the peak associated with the $C_6H_5O^+$ ion exhibited a shape which suggested that it resulted from two competitive unimolecular processes. Beynon et al. [3] proposed that the narrow component arose from an oxygen rearrangement to the ortho position prior to dissociation, and that the broad component was due to a three- or four-membered cyclic transition state by which the nitro group isomerised to the nitrite form.

In addition to the ion fragmentation studies, the present work includes a measurement of the absolute photoabsorption cross section of nitrobenzene between the ionisation threshold and 35 eV. As far as we are aware, these data represent the first photoabsorption measurements at energies above 8 eV [26,27].

2. Experimental apparatus and procedure

2.1. Mass spectrometry studies

The two-field time-of-flight mass spectrometer [25], in which the fragmentation study on nitrobenzene was carried out, and the 5 m normal incidence monochromator [28], attached to the Daresbury Laboratory synchrotron radiation source, have been described in detail previously so only a brief account will be given here. Photoionisation occurred in an interaction region, across which was applied a static electric field, and the electrons and ions traveled in opposite directions toward their respective channelplate detectors. The electrons passed through a simple lens system to maximise the collection efficiency but no kinetic energy analysis was performed. The time between the arrival of the electron and the associated ion was measured electronically, with the summation of many events producing a TOF spectrum. TOF spectra were recorded in the photon energy range 10–31 eV, and Fig. 1 shows the spectrum collected at 22.8 eV. Normalised relative abundance curves were obtained by integrating the peak area associated with each fragment ion and the parent ion.

2.2. Photoabsorption studies

The photoabsorption cross section was measured using a double ion chamber, and the experimental apparatus and procedure [29] have been described previously. The double ion chamber incorporated a set of plates, two of which were used to collect the photoions. At the rear of the chamber the transmitted radiation struck a sodium salicylate screen and the resulting fluorescence was detected with a photomultiplier. A lithium fluoride filter could be inserted into the photon beam to suppress higher-order radiation. A photoabsorption spectrum was measured by scanning the monochromator over the desired energy range and

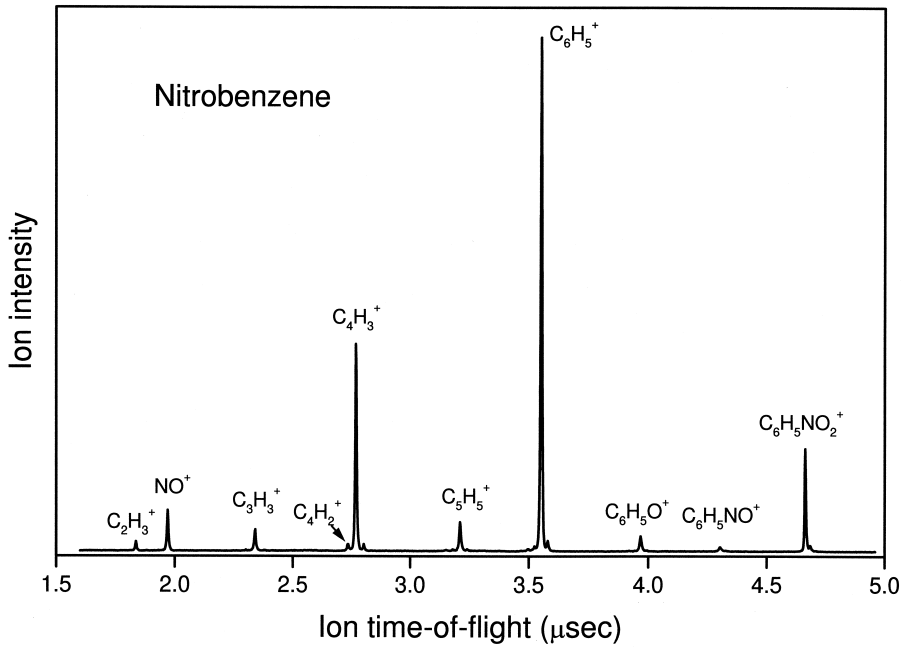

Fig. 1. Time-of-flight mass spectrum of nitrobenzene recorded at a photon energy of 22.8 eV.

recording the two electrometer currents, a reading proportional to the photomultiplier signal, and the gas pressure.

3. Results and discussion

3.1. Mass spectrometry studies

3.1.1. Overview

The relative abundance curves for the nitrobenzene parent and fragment ions are displayed in Figs. 2–6. Table 1 provides a summary of the experimental appearance energies for the main fragmentation processes, together with the values from previous investigations. The overall agreement is satisfactory. It should be noted that the differences between the values of the thermochemical thresholds estimated in the present work and those reported by Nishimura et al. [18] result from differences in the chosen heats of formation for particular ions or neutrals. The values given by Lias et al. [30] have been used in the present estimates.

At low energies the relative abundance curves demonstrate that the dissociation of the molecular ion is dominated by the production of $C_6H_5O^+$, $C_6H_5^+$, $C_5H_5^+$, and NO^+. However, at higher energies the formation of $C_4H_3^+$ and $C_3H_3^+$ becomes more important, together with a significant reduction in the intensity of $C_6H_5O^+$. As the thermodynamics of the fragment ions formed through processes (A)–(F) have been thoroughly discussed [15–20], the high intensity ions will be considered only briefly. The main emphasis will be placed on the low intensity ions which have received little attention in previous work and whose AEs are unknown. We will discuss all the fragment ions in decreasing mass order, and have presented a summary of the relevant information in Table 2. The following analysis is based primarily on a comparison between the experimentally measured AEs and the minimum energy requirement estimated from known thermochemical data. This analysis does not take reaction barriers into account, and it is not unusual for such barriers, for example to a ring opening or hydrogen migration, to have energies as

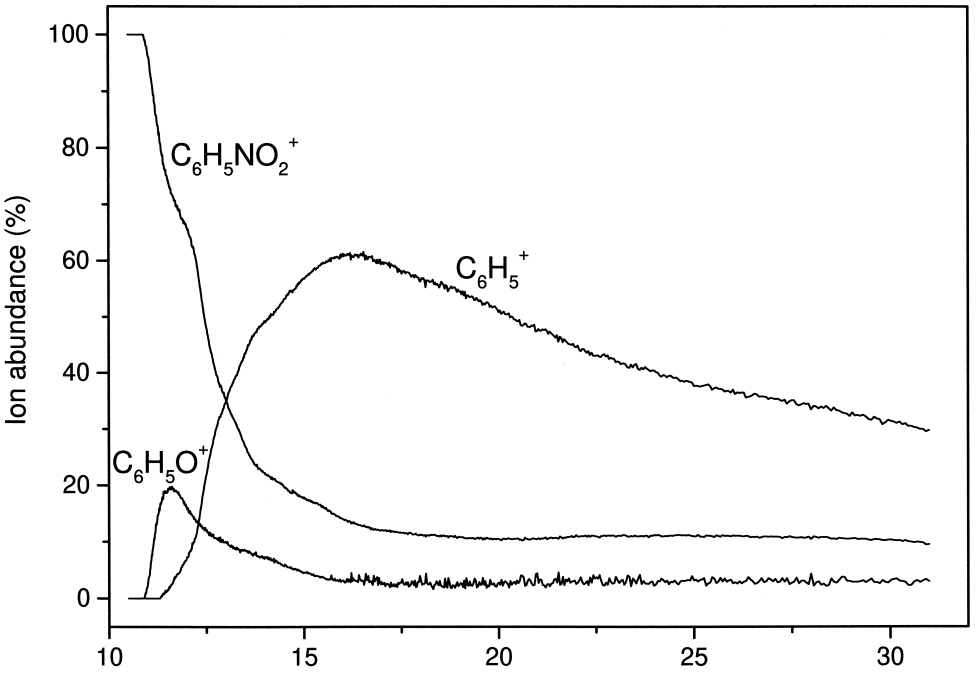

Fig. 2. Relative abundance curves for $C_6H_5NO_2^+$ (m/z = 123), $C_6H_5O^+$ (m/z = 93), and $C_6H_5^+$ (m/z = 77).

high as 1–2 eV. The reaction kinetics of the dissociation process are also important, and this effect will be apparent in cases where the most thermochemically favourable fragmentation process is kinetically unfavourable. Under such circumstances the observed AE will be higher than predicted. Table 3 gives, previously unknown, heats of formation for two ions derived from the experimental AEs.

3.1.2. Fragment ions

$C_6H_5NO^+$ (m/z = 107). The AE of this low intensity fragment was measured as 12.2 ± 0.2 eV, which is about 0.1 eV above the thermochemical threshold.

$C_6H_5O^+$ and $C_6H_5^+$ (m/z = 93 and 77). The high intensity fragmentation process (A), resulting in the formation of $C_6H_5O^+$ along with the elimination of neutral NO, is the lowest energy channel according to previous experimental work and known thermochemistry. The present AE of 10.9±0.1 eV is in excellent agreement with earlier investigations and is approximately 1.6 eV above the thermochemical threshold.

A similarly good agreement is obtained for process (B), which produces $C_6H_5^+$ and neutral NO_2. The AE of 11.3 ± 0.1eV indicates that this channel has a very small barrier. The dissociation mechanisms responsible for the formation of $C_6H_5O^+$ and $C_6H_5^+$ have been discussed at length [15–20]. Although the conclusion reached in the early TPEPICO study [16] was that the formation of $C_6H_5^+$ occurred from an excited electronic state, it now appears that the production of this ion occurs statistically from the ground electronic state [15].

$C_6H_4^+$, $C_6H_3^+$, and $C_6H_2^+$ (m/z = 76, 75, and 74). The $C_6H_4^+$ fragment, with an AE of 15 ± 1 eV, was observed very weakly even at high photon energies. This ion has not been included in the relative abundance curves.

The relatively high AEs of 19 ± 1 and 25.0 ± 0.5 eV, for the $C_6H_3^+$ and $C_6H_2^+$ fragments, respectively, indicate that these ions are being formed through sequential decompositions rather than arising directly from the molecular ion. In a sequential decomposi-

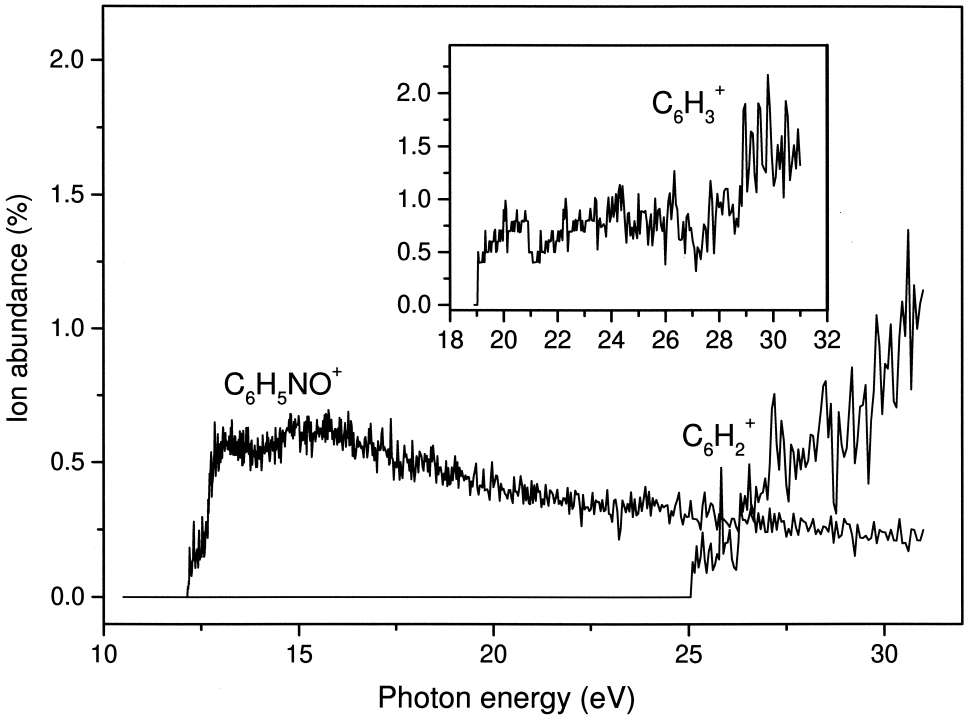

Fig. 3. Relative abundance curves for $C_6H_5NO^+$ (m/z = 107), $C_6H_3^+$ (m/z = 75), and $C_6H_2^+$ (m/z = 74).

tion, the final ionic and neutral products are not formed directly from the molecular ion through cleavage or rearrangement reactions, but are the end result of a number of sequential reactions in which atomic or small fragments are cleaved. A sequential decomposition is normally characterised by a high AE and a large number of small or atomic fragments, whereas production directly from the molecular ion usually results in a much lower AE and in the reaction products consisting mainly of stable molecular fragments.

The thermodynamics for the production of the $C_6H_3^+$ ion show that the mechanisms described by

$$C_6H_5NO_2^+ \rightarrow C_6H_3^+ + O_2 + H_2 + N \quad (1)$$

$$C_6H_5NO_2^+ \rightarrow C_6H_3^+ + NO_2 + 2H \quad (2)$$

give values of ~1430 kJ mol^{-1} for the upper limit of $\Delta H_f(C_6H_3^+)$ in both cases. As expected, this value lies between those of 1124.8 and 1565.1 kJ mol^{-1} for the $C_6H_5^+$ and $C_6H_2^+$ ions, respectively.

If the sequential decomposition mechanism given in process (2) is considered, then a comparable intensity of $C_6H_4^+$ would be expected. However, the $C_6H_4^+$ peak was extremely weak in the present investigation. This implies that atomic hydrogen is not produced and hence that the mechanism given in process (1), having a ΔH_f ($C_6H_3^+$) of ~1428 kJ mol^{-1}, is the more probable. It appears that energised $C_6H_5^+$, together with the N and O_2 neutrals, are created first, by way of a sequential decomposition, followed by the elimination of H_2 to produce the observed $C_6H_3^+$ fragment. It should be noted that the proposed sequential decomposition, summarised by process (2), for the formation of $C_6H_3^+$ does not imply that the four-body reaction producing this ion was actually observed in the present experimental investigation. Rather, the basis for the proposed mechanism lies on energetic considerations derived from thermodynamic estimates. The energetics indicate the process (2) is the more likely mechanism, thereby suggesting that $C_6H_3^+$ production occurs by means of a four-body reaction.

It is interesting to compare the formation of the

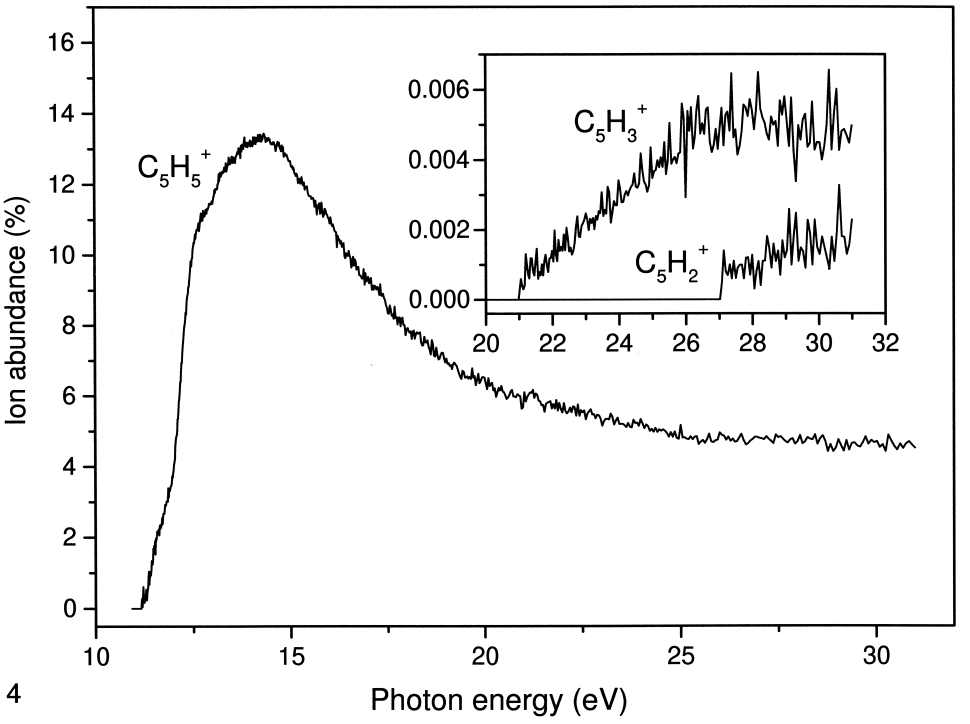

Fig. 4. Relative abundance curves for $C_5H_5^+$ (m/z = 65), $C_5H_3^+$ (m/z = 63), and $C_5H_2^+$ (m/z = 62).

$C_6H_5^+$ ion through the sequential process (1) with its formation through the cleavage mechanism given in process (B). Production by way of process (1) occurs at a characteristically high AE and is accompanied by atomic fragments. In contrast, fragmentation channel (B) with a low AE of 11.3 eV, produces the $C_6H_5^+$ fragment along with molecular NO_2.

Similar mechanisms, given in

$$C_6H_5NO_2^+ \rightarrow C_6H_2^+ + O_2 + H_2 + N + H \quad (3)$$

$$C_6H_5NO_2^+ \rightarrow C_6H_2^+ + NO_2 + 3H \quad (4)$$

may be applied to the formation of $C_6H_2^+$, and both yield thermochemical thresholds of ~22.6 eV. However, invoking the same arguments that have been discussed in relation to the production of $C_6H_3^+$, the formation of $C_6H_2^+$ by way of process (4) would be expected to yield a higher intensity of $C_6H_4^+$ than was observed experimentally. This evidence suggests that process (3) is the more probable.

As in the case of $C_6H_3^+$ production, the proposal that the $C_6H_2^+$ fragment is formed through process (3) does not imply that the many-body decomposition process was observed directly in the experiment.

$C_5H_5^+$, $C_5H_4^+$, $C_5H_3^+$, and $C_5H_2^+$ (m/z = 65, 64, 63, and 62). The AE of the prominent $C_5H_5^+$ fragment was measured as 11.2 ± 0.2 eV, which is in good agreement with previous results and is 1.2 eV above the thermochemical threshold. $C_5H_5^+$ is produced via $C_6H_5O^+$ by two consecutive reactions involving firstly the loss of NO followed by the loss of CO. The formation of this ion has been discussed in detail previously [15,16,18].

The $C_5H_4^+$ fragment, with an AE of 18 ± 1 eV, was observed weakly. This ion has not been included in the relative abundance curves.

The AEs for the low intensity $C_5H_3^+$ and $C_5H_2^+$ fragments were measured as 21.0 ± 0.5 and 27 ± 1 eV, respectively. The high AEs for these two ions suggest that they are being formed through sequential

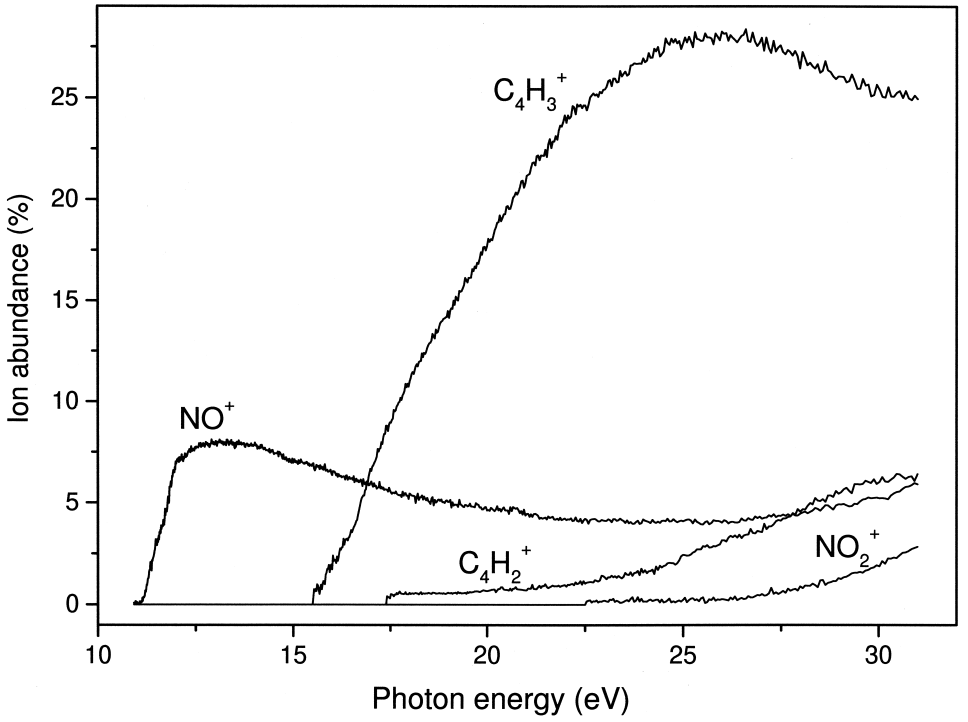

Fig. 5. Relative abundance curves for $C_4H_3^+$ ($m/z = 51$), $C_4H_2^+$ ($m/z = 50$), NO_2^+ ($m/z = 46$), and NO^+ ($m/z = 30$).

decomposition mechanisms. There are six possible reactions for each ion, all of which give reasonable values for the heats of formation. However, the production of $C_5H_2^+$ plus atomic carbon from $C_6H_2^+$, where the $C_6H_2^+$ ion is being formed through process (3) or (4), yields quite reasonable values for ΔH_f ($C_5H_2^+$) of ~1270 kJ mol^{-1}. As already discussed, processes (3) and (4) result in thermochemical thresholds for the production of $C_6H_2^+$ that are closest to the experimental AE for this fragment. Thus, it appears reasonable to propose that the formation of $C_5H_2^+$ occurs from a $C_6H_2^+$ fragment created by process (3) or (4). The same argument cannot be applied to the formation of the $C_5H_3^+$ fragment from the $C_6H_3^+$ ion as this would result in a heat of formation which is far too low. All the possible fragmentation reactions which could produce $C_5H_3^+$ include the elimination of one or two neutral molecules.

$C_4H_3^+$ and $C_4H_2^+$ (m/z = 51 and 50). Fragmentation channel (D) produces $C_4H_3^+$ with a high intensity. The AE of this ion was measured to be 15.5 ± 0.2 eV, which is in good agreement with the value of 15.66 ± 0.15 eV obtained by Nishimura et al. [18]. These findings are in contrast with those reported by Panczel and Baer [16] who observed $C_4H_3^+$ between 11.4 and 12.65 eV, and gave the AE as 11.40 ± 0.05 eV. The $C_4H_3^+$ ion may be produced from nitrobenzene in the following fragmentation processes:

$$C_6H_5NO_2^+ \rightarrow C_6H_5O^+ + NO \rightarrow C_4H_3^+ + NO + C_2H_2O \quad (5)$$

$$C_6H_5NO_2^+ \rightarrow C_6H_5^+ + NO_2 \rightarrow C_4H_3^+ + NO_2 + C_2H_2 \quad (6)$$

Nishimura et al. used a heat of formation of 1284 kJ mol^{-1} for the $C_4H_3^+$ ion, derived from an electron impact study on vinylacetylene [31]. This led to estimated thermochemical thresholds of 12.94 eV for process (5) where the $C_4H_3^+$ ion is formed by the elimination of C_2H_2O from $C_6H_5O^+$, and of 15.33 eV

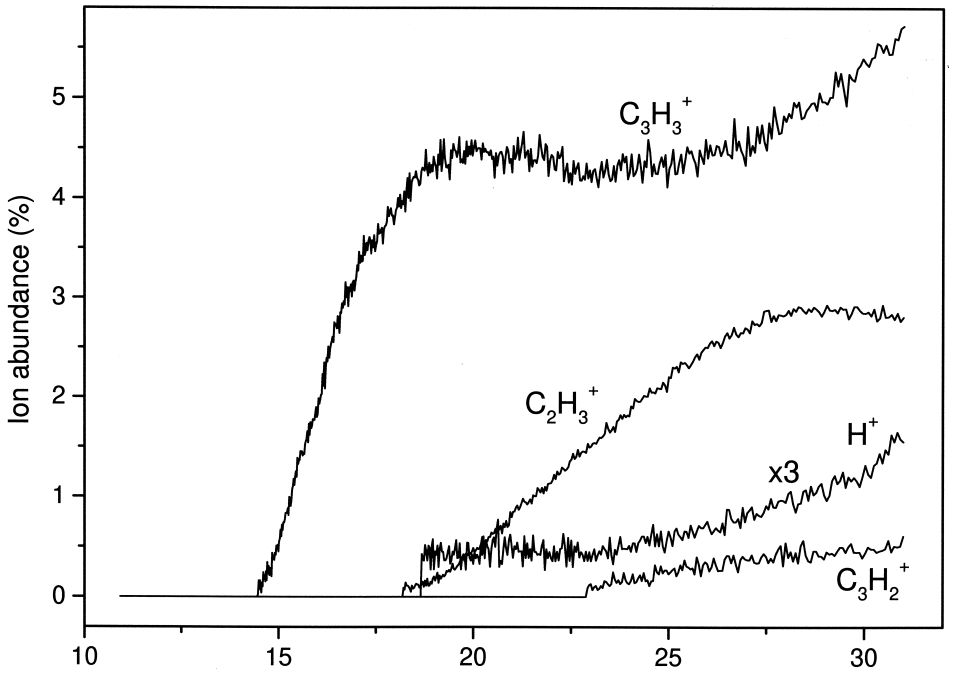

Fig. 6. Relative abundance curves for $C_3H_3^+$ (m/z = 39), $C_3H_2^+$ (m/z = 38), $C_2H_3^+$ (m/z = 27), and H^+ (m/z = 1).

for process (6) where the ion is formed by the elimination of C_2H_2 from $C_6H_5^+$. As the AE of 11.40 eV, measured by Panczel and Baer, lies far below the lowest thermochemical threshold, when based on ΔH_f ($C_4H_3^+$) = 1284 kJ mol^{-1}, these authors [16] suggested that the heat of formation for $C_4H_3^+$ derived from the electron impact study represented an upper limit, implying that the estimated thresholds of 12.94 and 15.33 eV also represented upper limits. Panczel and Baer proposed two alternative values for the heat of formation of $C_4H_3^+$. The first was obtained by combining an appearance energy measured by Dannacher [32] with the heat of formation of the neutral molecule [33]. This resulted in ΔH_f ($C_4H_3^+$) = 1272 kJ mol^{-1}. Their second estimate was obtained by combining heats of formation for C_4H_2 and a hydrocarbon group value with the ionisation energy of neutral C_4H_3. This gave a ΔH_f ($C_4H_3^+$) of 1165 kJ mol^{-1} [16]. The lowest thermochemical threshold for process (5), based on the ΔH_f ($C_4H_3^+$) of 1165 kJ mol^{-1}, is 11.8 eV. An estimation based on the present AE yields an upper limit for ΔH_f ($C_4H_3^+$) of 1302 kJ mol^{-1}. As a value of 1165 kJ mol^{-1} would be expected to be approximately correct, it appears that this fragmentation channel contains some rather large barriers.

The AE of $C_4H_2^+$ has been measured as 17.5 ± 0.5 eV, indicating that this ion is being formed through a sequential fragmentation process. If it is assumed that the ion has the 1,3 butadiyne linear structure with a ΔH_f ($C_4H_2^+$) of 1420.6 kJ mol^{-1}, then the following fragmentation channels, with thermochemical thresholds of 16.74 and 17.12 eV, respectively, are the most probable:

$$C_6H_5NO_2^+ \rightarrow C_4H_2^+ + NO + C_2H_2O + H \quad (7)$$

$$C_6H_5NO_2^+ \rightarrow C_4H_2^+ + NO_2 + C_2H_3 \quad (8)$$

Channel (7) is similar to channel (5), but with the additional loss of a hydrogen atom from the $C_4H_3^+$ ion.

However, it is possible that the lowest energy fragmentation channel, producing neutral NO, CO, and CH_3, and having a thermochemical threshold of 15.34 eV, contains a large barrier. If this is the case,

Table 1
Appearance energies and thermochemical thresholds for reactions (A)–(F)

	Appearance energy (eV)		Thermochemical threshold (eV)	
Reactions	Previous work	This work	Nishimura et al. [18]	This work
(A) $C_6H_5O^+ + NO$	10.98,[a] 10.89[b] 10.95,[c] 10.41[d] 10.35,[e] 10.1[f]	10.9 ± 0.1	9.33	9.33
(B) $C_6H_5^+ + NO_2$	11.14,[a] 11.08,[b] 11.15,[c] 11.66,[d] 11.93,[e] 11.2,[f] 12.14[g]	11.3 ± 0.1	11.15	11.3
(C) $C_5H_5^+ + CO + NO$	11.30,[a] 11.08,[b] 10.8[f]	11.2 ± 0.2	10.32	10.03
(D) $C_4H_3^+ + (NO + C_2H_2O)/(NO_2 + C_2H_2)$	11.40,[a] 15.66,[b] 14.4,[f] 16.31[g]	15.5 ± 0.2	12.94 (15.33)	See text for details
(E) $C_3H_3^+ + NO + CO + C_2H_2$	12.63[b]	14.5 ± 0.2	12.61	12.6–13.9 (see Table 2)
(F) $NO^+ + C_6H_5O$	11.04,[a] 10.89[b]	10.9 ± 0.2	10.02	10.0

[a] See [16].
[b] See [18].
[c] See [7].
[d] See [1].
[e] See [2].
[f] See [5].
[g] See [12].

then its contribution might not be observed below 17.4 eV.

NO_2^+ (m/z = 46). The NO_2^+ ion was observed only at energies above 26 eV. This suggests that it is not being formed, along with the neutral phenyl radical C_6H_5, by way of the low energy fragmentation channel which has a thermochemical threshold of 12.64 eV. Several possible mechanisms, all of which involve neutral molecules, are listed in Table 2. However, the high AE indicates that this ion is formed after several sequential decompositions, where small parts of the carbon backbone are lost, rather than by elimination of stable C_2H_2 and C_3H_n neutrals.

Very little information is available concerning the formation of NO_2^+ from the nitrobenzene ion, and it appears only very weakly in the standard 70 eV electron impact mass spectrum [9]. This fragment provides a good example of Stevenson's rule [34], which states that in any ion dissociation producing two different products, the charge generally resides on the fragment of lower ionisation energy. Even where it is possible to observe the fragment with the higher ionisation energy with a reasonable yield, the threshold measured is often far higher that the thermochemically derived threshold. Hence, for nitrobenzene, for energies below 26 eV an ionic hydrocarbon fragment would be preferred to the production of NO_2^+. We have observed similar behaviour in furan [22] and toluene [25].

Fig. 7 shows examples of the time-of-flight peaks associated with the NO^+ and the NO_2^+ ions recorded at various photon energies. The width of the peak is dependent, amongst other parameters, on the initial kinetic energy possessed by the ion. The shortest flight time is given by ions created with their initial

Table 2
Fragment ion appearance energies and the most pertinent thermochemical thresholds

m/z	Fragment	AE(eV)	Thermochemical thresholds (eV)
107	$C_6H_5NO^+ + O$	12.2 ± 0.2	12.06
93	$C_6H_5O^+ + NO$	10.9 ± 0.1	9.33
	$C_6H_5O^+ + N + O$		16.3
77	$C_6H_5^+ + NO_2$	11.3 ± 0.1	11.3
	$C_6H_5^+ + N + O_2$		15.8
76[a]	$C_6H_4^+$	15 ± 1	
75	$C_6H_3^+$	19 ± 1	
74	$C_6H_2^+ + NO_2 + H_2 + H$	25.0 ± 0.5	18.13
	$C_6H_2^+ + N + O_2 + H_2 + H$		22.68
	$C_6H_2^+ + NO_2 + 3H$		22.64
	$C_6H_2^+ + N + 2O + H_2 + H$		27.85
65	$C_5H_5^+ + NO + CO$	11.2 ± 0.2	10.03
	$C_5H_5^+ + CN + O_2$		14.73
64[a]	$C_5H_4^+$	18 ± 1	
63	$C_5H_3^+$	21.0 ± 0.5	
62	$C_5H_2^+$	27 ± 1	
51	$C_4H_3^+ + NO + C_2H_2O$	15.5 ± 0.2	
	$C_4H_3^+ + NO_2 + C_2H_2$		
50	$C_4H_2^+ + NO + CO + CH_3$	17.5 ± 0.5	15.34
	$C_4H_2^+ + NO + C_2H_2O + H$		16.74
	$C_4H_2^+ + NO_2 + C_2H_3$		17.12
	$C_4H_2^+ + NO_2 + C_2H_2 + H$		18.99
	$C_4H_2^+ + NO + O + C_2H_3$		20.30
	$C_4H_2^+ + NO + O + C_2H_2 + H$		22.18
	$C_4H_2^+ + N + O + C_2H_2O + H$		23.27
	$C_4H_2^+ + CN + O_2 + CH_2 + H$		24.83
46	$NO_2^+ + C_6H_5$	26 ± 1	12.64
	$NO_2^+ + (cyclo\text{-})C_3H_2 + C_3H_3$		(15.60) 14.79
	$NO_2^+ + (cyclo\text{-})C_3H_2 + cyclo\text{-}C_3H_3$		(16.63) 15.81
	$NO_2^+ + H + 2(cyclo\text{-})C_3H_2$		(17.18) 15.54
	$NO_2^+ + CH + C_2H_2 + (cyclo\text{-})C_3H_2$		(20.60) 19.79
39	$(cyclo\text{-})C_3H_3^+ + NO + CO + C_2H_2$	14.5 ± 0.2	(12.63) 13.67
	$(cyclo\text{-})C_3H_3^+ + NO_2 + C_3H_2$		(12.83) 13.87
	$(cyclo\text{-})C_3H_3^+ + NO_2 + cyclo\text{-}C_3H_2$		(13.65) 14.69
38	$(cyclo\text{-})C_3H_2^+ + NO + CO + C_2H_3$	23 ± 1	(13.85) 14.31
	$(cyclo\text{-})C_3H_2^+ + NO_2 + C_3H_3$		(15.17) 15.63
	$(cyclo\text{-})C_3H_2^+ + NO_2 + cyclo\text{-}C_3H_3$		(16.20) 16.66
	$(cyclo\text{-})C_3H_2^+ + NO + O + C_3H_3$		(18.36) 18.82
	$(cyclo\text{-})C_3H_2^+ + NO + O + cyclo\text{-}C_3H_3$		(19.38) 19.84
	$(cyclo\text{-})C_3H_2^+ + NO + O + C_2H_2 + CH$		(23.36) 23.82
30	$NO^+ + C_6H_5O$	10.9 ± 0.2	10.0
	$NO^+ + C_6H_5 + O$		15.5
27	$C_2H_3^+ + NO + CO + (cyclo\text{-})C_3H_2$	18.2 ± 0.5	(12.95) 12.13
	$C_2H_3^+ + NO_2 + C_4H_2$		15.20
	$C_2H_3^+ + NO + O + C_4H_2$		18.38
	$C_2H_3^+ + NO_2 + (cyclo\text{-})C_3H_2 + CH$		(19.66) 18.85
1	H^+	19 ± 1	

[a] These masses were observed at very low intensity and have not been included in the relative abundance curves.

Table 3
New upper limits for the heats of formation of fragment ions, derived from the experimental measurements

Fragment	ΔH_f (kJ mol^{-1})
$C_6H_3^+$	1428
$C_5H_2^+$	1270

velocity directed along the spectrometer axis and towards the detector. Conversely, the longest flight time is given by ions created with their initial velocity directed away from the detector. These ions begin traveling away from the TOF drift tube, are turned around by the electric field, and subsequently travel towards the detector.

Within the experimental uncertainty, the width of the NO_2^+ peak, and consequently the initial kinetic energy possessed by the NO_2^+ fragment, remains constant as a function of photon energy. If it is assumed that the base width can be attributed to energetic ions traveling initially either directly toward or away from the detector, then an analysis of the TOF peak shape shows that the initial maximum translational energy possessed by the NO_2^+ ion is about 2.8 eV. Over the entire photon energy range in which the NO_2^+ peak was observed, its width was always large. The large width is apparent when a comparison is made with the peak associated with the NO^+ ion. Fig. 7 illustrates that, at high photon energy, the NO^+ peak appears to be composed from two contributions. The first contribution is due to ions having low initial kinetic energies and is responsible for the narrow, central component in the TOF peak. At low photon energies, this component is the only one observed. Fig. 7 shows the NO^+ peak recorded at a photon energy of 25 eV where only the single, narrow component is present. This narrow component may be regarded as having a width typical of that for a singly charged ion formed through a fragmentation process in which only one ion is produced. The second contribution is caused by energetic ions and gives rise to a substantial increase in the peak base width. It is apparent that the width of the peak associated with the NO_2^+ fragment is always significantly broader than the central component in the NO^+ peak.

The doubly charged parent ion was not observed in

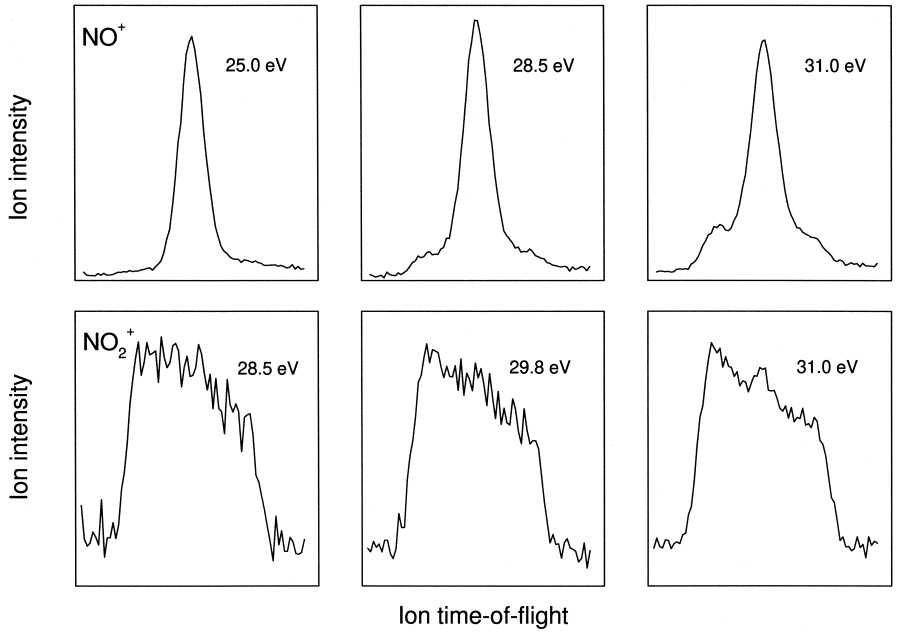

Fig. 7. Upper three frames: time-of-flight peak associated with the NO^+ fragment, recorded at photon energies of 25.0, 28.5, and 31.0 eV. Lower three frames: time-of-flight peak associated with the NO_2^+ fragment recorded at photon energies of 28.5, 29.8, and 31.0 eV.

the present study, and, to the best of our knowledge, the double ionisation threshold of nitrobenzene has not been established. However, those of benzene and toluene are 24.6 [35] and 23.8 eV [25], respectively. Therefore it is not unreasonable to anticipate that the double ionisation threshold of nitrobenzene lies in the energy region in which the NO^+ peak begins to exhibit an increase in base width. It appears that the doubly charged ion is unstable, at least with respect to the microsecond timescale relevant to the present study, and forms two singly charged species and possibly one or more neutral fragments.

The initial maximum translational energy (~2.8 eV) possessed by the NO_2^+ ion is significantly greater than that released in a typical unimolecular decomposition. A translational energy of such magnitude must arise through the coulomb repulsion of two positive ions. If it is assumed that one of the charges resides on the phenyl ring and the other on the NO_2 fragment, then the fragments will repel one another and a measurement of the kinetic energy carried by one of the ions will allow the initial ion–pair separation (r) to be determined. In a simple coulomb explosion model [36], the dissociation energy (E) is related to the initial separation by E (eV) = $14.4q_1q_2/r$ (Å), where q_1 and q_2 are the charges (in coulombs) on the two ions. Assuming that dissociation of the doubly charged parent ion produces only NO_2^+ and $C_6H_5^+$, so that no consideration needs to be given to an additional neutral fragment, then conservation of momentum results in a total dissociation energy of 4.5 eV. This energy leads to an ion-pair separation of 3.2 Å if $q_1 = q_2 = 1$. As expected, the value of r obtained from the peak width analysis is larger than the C-N bond length (~1.03 Å [37]) in nitrobenzene. This dissimilarity may be reconciled in a qualitative manner by considering the following two points. First, q_1 and q_2 will be less than unity due to the shielding effects of the surrounding electrons. Second, the charge on the ring will be delocalised rather than concentrated solely on the carbon atom closest to the NO_2 fragment. As the distance between the nitrogen atom and the furthest carbon atom is ~3.2 Å [37], it appears that both of these effects may be required to account for the present results.

It is noticeable that the NO_2^+ peak recorded at a photon energy of 31 eV exhibits a central narrow spike superimposed upon the broad trapezoid. This central feature can be attributed to NO_2^+ ions, having low initial kinetic energies, created through decompositions forming only one singly charged ion.

$C_3H_3^+$ and $C_3H_2^+$ (m/z = 39 and 38). The AE of the prominent $C_3H_3^+$ fragment, formed through process (E), was measured as 14.5 ± 0.2 eV. Our AE does not agree with the value of 12.63 eV reported by Nishimura et al.[18]. The low AE measured by Nishimura et al. led them to the conclusion that the $C_3H_3^+$ fragment was being formed from $C_5H_5^+$ because their AE lay close to the thermochemical threshold for this process (Table 2). However, Panczel and Baer [16] did not observe the $C_3H_3^+$ ion in the photon energy range 10–13.3 eV covered in their experiment.

The high AE of 23 ± 1 eV for the low intensity $C_3H_2^+$ ion indicates that it is being formed through sequential decomposition processes. The likely fragmentation processes, all of which involve the elimination of molecules as the neutral products, are listed in Table 2. From these mechanisms the most probable is the following fragmentation process

$$C_6H_5NO_2^+ \rightarrow (\text{cyclo-})C_3H_2^+ + NO + O + (\text{cyclo-})C_3H_3 \quad (9)$$

The estimated thermochemical thresholds lie between 18.36 and 19.84 eV, and depend upon the structures of the $C_3H_2^+$ ion and the C_3H_3 neutral, both of which can take either planar or cyclic forms.

NO^+ (m/z = 30). In agreement with earlier work [16,18] the NO^+ fragment, arising through process (F), was observed at 10.9 ± 0.2 eV. This AE lies 0.9 eV above the thermochemical threshold. Previous studies [15,16,18] have established that this ion is formed statistically, via a rearrangement process, as the thermochemical threshold for direct cleavage from the molecular ion, which results in the neutral products C_6H_5 and O, is 15.5 eV.

The TOF peak associated with the NO^+ ion exhibits an interesting change in shape as a function

of photon energy. For incident energies between 10.9 and ~25 eV the peak is relatively narrow and has a width similar to those associated with adjacent ions. However, for energies above 25 eV a second, and substantially broader, component begins to develop, and by 31 eV the NO^+ peak clearly contains contributions from two sources (Fig. 7). The high kinetic energy, broad, component can be attributed to the decomposition of a doubly charged ion into two singly charged species, one of which is NO^+. An analysis of the NO^+ peak width, using the procedure already described for the NO_2^+ ion, indicates that the initial, maximum, kinetic energy possessed by the energetic ions is about 4.2 eV. If it is assumed that no neutral fragment is generated in the dissociation of the doubly charged parent ion, then this energy corresponds to an ion–pair separation of 2.6 Å.

Kinetic energy release distributions for the NO^+ fragment were measured in the TPEPICO experiments [16,18], and Panczel and Baer report an average kinetic energy release of 0.045 eV. These low energy fragments are responsible for the narrow component observed in the NO^+ TOF peak. The photon energy at which the broad component first appears provides an estimate of the double ionisation threshold of nitrobenzene. The present results indicate an upper limit of 27.9 eV for this threshold.

Fig. 7 shows that at a photon energy of 31 eV the peaks associated with the NO^+ and the NO_2^+ ions exhibit contrasting shapes. The dominant contribution to the NO^+ peak arises from ions created in processes forming a single ion with low kinetic energy. The contribution due to energetic ions is relatively weak. On the other hand, the NO_2^+ peak displays a broad trapezoidal shape, attributable to energetic ions produced in a coulomb explosion of a doubly charged molecular ion. The central, narrow component is barely discernible.

$C_2H_3^+$ and H^+ (m/z = 27 and 1). Various fragmentation channels which could produce the low intensity $C_2H_3^+$ ion, with an AE of 18.2 ± 0.5 eV, have been summarised in Table 2. Formation through the process with a thermochemical threshold at 15.2 eV seems most likely, but the experimental uncertainty is such that the higher energy channel with a threshold at 18.38 eV cannot be discounted.

The AE of the H^+ ion from nitrobenzene was found to be 19 ± 1 eV.

Table 4
A summary of the appearance energies of the hydrocarbon fragments produced upon outer valence shell photoionisation of nitrobenzene, benzene, and toluene, to illustrate the influence of the substituent

		Appearance energies (eV)		
Ions	Fragment	Nitrobenzene[a]	Benzene[b]	Toluene[c]
1	$C_6H_5^+$	11.3	14.0 (12.90[d])	14.4
2	$C_6H_4^+$	15	14.3 (12.93[d])	20.7
3	$C_6H_3^+$	19	21.8	21.0
4	$C_6H_2^+$	25.0	23.8	24.8
5	$C_5H_5^+$	11.2		16.5
6	$C_5H_4^+$	18		17.2
7	$C_5H_3^+$	21.0	15.7	17.6
8	$C_5H_2^+$	27	19.1	23.8
9	$C_4H_3^+$	15.5	17.5	17.8
10	$C_4H_2^+$	17.5	17.7	19.1
11	$C_3H_3^+$	14.5	14.8 (13.43[d])	17.5
12	$C_3H_2^+$	23	22.8	21.0
13	$C_2H_3^+$	18.2	18.9	18.2

[a] This work.
[b] See [21].
[c] See [25].
[d] See [38]. Results from multiphoton excitation study.

3.1.3. Comparison of fragment ion appearance energies in benzene, toluene and nitrobenzene

The nitro substituent is electron poor compared to the benzene ring and destabilises the π ring system by withdrawing electron density in attempting to form the fully delocalised system O=N=O. In contrast, the methyl substituent on the benzene ring in toluene stabilises the ring by donating electrons into the σ system. The effect of this electron transfer should manifest itself in the fragmentation patterns. One way to investigate this influence is through a comparison of the AEs of the various hydrocarbon ions. The AEs of the fragment ions derived from the photoionisation studies of benzene [21], toluene [25] and nitrobenzene are listed in Table 4, and the fragments have been numbered 1–13 to simplify the discussion. Also included in Table 4 are AEs of fragment ions derived in a multiphoton excitation experiment on benzene per-

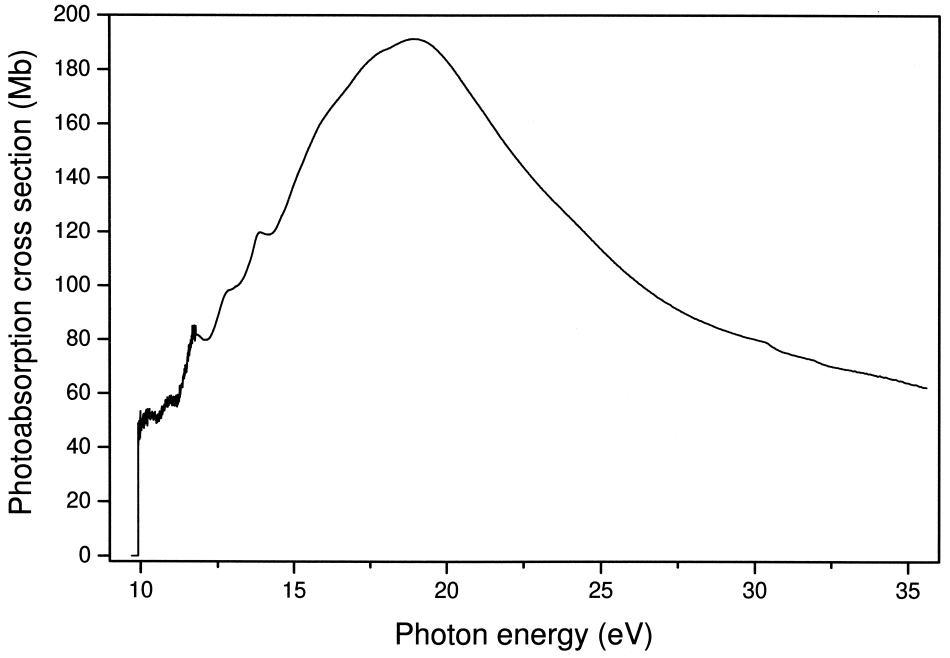

Fig. 8. Total photoabsorption cross section of nitrobenzene.

formed by Kuhlewind et al. [38]. The results for benzene and the influence of the kinetic shift, have been discussed by Holland et al. [21].

It should be borne in mind that a meaningful comparison amongst the AEs can only be carried out when the hydrocarbon fragments are being produced via a similar mechanism. If the production of a certain fragment involves a rearrangement, which is specific to that particular parent ion, then this may lead to a low AE in only one of the three ring systems. Under such circumstances the comparison will not be valid.

The dependence of the AEs on the stability of the different ring systems is illustrated by fragments 1, 9, and 10. The AEs of these three fragments decrease according to the trend toluene > benzene > nitrobenzene. In the cleavage reaction

$$C_6H_5X^+ \rightarrow C_6H_5^+ + X$$

where X = NO_2, CH_3, or H, it would be expected that the AEs directly reflect the stability of the rings. Table 4 shows that the AE of the $C_6H_5^+$ ion is 11.3, 14.0 (12.90), and 14.4 eV in nitrobenzene, benzene, and toluene, respectively. These AEs are in accordance with the electron donating or withdrawing character of the substituent. The CH_3 group, which exerts a small positive mesomeric effect on the ring, results in an AE for the $C_6H_5^+$ fragment from toluene which is higher than that found in benzene. Conversely, the NO_2 group, which exerts a larger negative inductive effect, leads to an AE which is substantially lower than that found in benzene. Fragments 3, 4, 6, 12, and 13, which are produced through sequential decompositions, have AEs, which do not appear to depend greatly on the stability of the ring system. However, in some cases, the intermediate ion in a sequential decomposition is clearly influencing the AE of a particular fragment, and is disturbing the general trend. The effect of the intermediate ion can be seen in the AEs for fragments 2, 7, 8, and 11.

3.2. Photoabsorption studies

Fig. 8 displays the absolute photoabsorption cross section of nitrobenzene between the ionisation thresh-

old and 35 eV, and the prominent broad features are somewhat similar to those observed in the spectra of the related molecules benzene [39] and toluene [25]. These latter two molecules also display sharp structure, which can be attributed to transitions into Rydberg states. This is not the case with nitrobenzene and the absence hampers the interpretation of the spectrum. Another difficulty stems from the uncertainty in the ground state molecular orbital sequence. Recent theoretical work by Takezaki et al. [40] suggests that the ground state is mainly described by the electronic configuration (in C_{2v} symmetry)

$$\ldots (1b_1)^2(2b_1)^2(16a_1)^2(11b_2)^2(1a_2)^2(3b_1)^2(2a_2)^2\ {}^1A_1$$

The three lowest lying virtual orbitals are predicted as $4b_1$, $3a_2$, and $5b_1$, where the $4b_1$ and $3a_2$ orbitals are derived from the $1e_{2u}$ orbital of benzene, and $5b_1$ is derived from $1b_{2g}$.

The HeI excited photoelectron spectrum of nitrobenzene has been recorded [41–48] but none of the bands, apart from that corresponding to ionisation from the $2a_2$ orbital, exhibits vibrational structure. The Penning ionisation spectrum has also been measured [49] and is similar to the photoelectron spectrum. The lack of vibrational progressions, and the overlap between the electronic bands, has hindered the experimental verification of the molecular orbital configuration. Photoelectron angular distributions have been determined by Katsumata et al. [47], and these have allowed some tentative orbital assignments to be proposed, based upon the β values. The assignments for the five outermost orbitals suggested by Katsumata et al. [47] are similar, but not identical, to those predicted by Takezaki et al. [40].

Electron energy loss spectra of nitrobenzene have been recorded in the vicinity of the C, N, and O *K*-shell edges [50] and for the valence shell [51]. These spectra have been determined under conditions that should simulate photon absorption. Therefore the valence shell spectrum measured by Ari et al. [51] should be identical to the present data. However, a comparison shows that the spectra are different both in general shape and in the relative prominence of the broad features.

Ari et al. have assigned some very weak and broad features to an *s*-type Rydberg series converging onto an ionisation limit at 13.5 eV. The present spectrum, which displays more well developed peaks, provides little support for this interpretation. All the features observed by Nagakura et al. [26] in the absorption spectrum below the ionisation threshold were broad and exhibited no sharp structure. No Rydberg series were identified [26]. Indeed, Robin [52] has assigned all the features appearing below the ionisation threshold to transitions localised within either the ring or the nitro group, and to additional charge transfer excitations between these moieties.

Rydberg structure was also very weak in the innershell spectra recorded by Turci et al. [50]. These spectra were dominated by a single intense peak, located 6–8 eV below the C, N, or O *K*-shell edges, which was attributed to transitions into the $\pi^*(4b_1)$, $\pi^*(5b_1)$, or π^*_{NO} orbitals.

Theoretical work [26,40,53,54] has been carried out to investigate the electronic transitions that occur at excitation energies below 8 eV, and these predictions have been used to interpret some of the experimental features. However, none of the calculations extends above the ionisation threshold, and into the energy region relevant to the present work.

The structure observed in the absorption spectrum (Fig. 8) appears too broad to be associated with transitions into Rydberg states. A more attractive interpretation seems to involve valence shell transitions into π^* orbitals. The corresponding transitions in the *K* shell excitation spectra give rise to intense peaks [50]. Taking into account the tendency for valence shell excitations to move a few electron volts toward higher energy compared to *K*-shell locations, it is conceivable that transitions into π^* orbitals give rise to the broad features observed around 10.2, 10.9, 11.7, 12.8, and 13.8 eV. This interpretation is supported by evidence from the photoelectron spectrum, which exhibits prominent bands at the appropriate binding energies. Nevertheless, such proposals are speculative and a proper interpretation must await theoretical guidance.

Acknowledgements

The authors are grateful for financial support and a CASE studentship (L.C.) from the EPSRC, and for a Visiting Fellowship (L.G.S.) from the Royal Society.

References

[1] P. Brown, Org. Mass Spectrom. 3 (1970) 1175.
[2] P. Brown, Org. Mass Spectrom. 4 (1970) 533.
[3] J.H. Beynon, M. Bertrand, R.G. Cooks, J. Am. Chem. Soc. 95 (1973) 1739.
[4] E.G. Jones, L.E. Bauman, J.H. Beynon, R.G. Cooks, Org. Mass Spectrom. 7 (1973) 185.
[5] F.W. McLafferty, P.F. Bente, R. Kornfeld, S.-C. Tsai, I. Howe, J. Am. Chem. Soc. 95 (1973) 2120.
[6] D. Cameron, J.E. Clark, T.L. Kruger, R.G. Cooks, Org. Mass Spectrom. 12 (1977) 111.
[7] V.M. Matyuk, V.K. Potapov, A.L. Prokhoda, Russ. J. Phys. Chem. 53 (1979) 538.
[8] E.S. Mukhtar, I.W. Griffiths, F.M. Harris, J.H. Beynon, Org. Mass Spectrom. 15 (1980) 51.
[9] C.J. Proctor, B. Kralj, A.G. Brenton, J.H. Beynon, Org. Mass Spectrom. 15 (1980) 619.
[10] C.J. Porter, J.H. Beynon, T. Ast, Org. Mass Spectrom. 16 (1981) 101.
[11] I.W. Griffiths, E.S. Mukhtar, F.M. Harris, J.H. Beynon, Int. J. Mass Spectrom. Ion Phys. 38 (1981) 333.
[12] S.H. Allam, M.D. Migahed, A. El-Khodary, Int. J. Mass Spectrom. Ion Phys. 39 (1981) 117.
[13] S.H. Allam, M.D. Migahed, A. El-Khodary, Egypt. J. Phys. 13 (1982) 167.
[14] E.E. Kingston, T.G. Morgan, F.M. Harris, J.H. Beynon, Int. J. Mass Spectrom. Ion Phys. 47 (1983) 73.
[15] W.G. Hwang, M.S. Kim, J.C. Choe, J. Phys. Chem. 100 (1996) 9227.
[16] M. Panczel, T. Baer, Int. J. Mass Spectrom. Ion Phys. 58 (1984) 43.
[17] T.L. Bunn, A.M. Richard, T. Baer, J. Chem. Phys. 84 (1986) 1424.
[18] T. Nishimura, P.R. Das, G.G. Meisels, J. Chem. Phys. 84 (1986) 6190.
[19] M. Moini, J.R. Eyler, Int. J. Mass Spectrom. Ion Phys. 76 (1987) 47.
[20] T.H. Osterheld, T. Baer, J.I. Brauman, J. Am. Chem. Soc. 115 (1993) 6284.
[21] D.M.P. Holland, D.A. Shaw, M.A. Hayes, I. Sumner, L. Cooper, E.E. Rennie, J.E. Parker, C.A.F. Johnson, to be published.
[22] E.E. Rennie, C.A.F. Johnson, J.E. Parker, D.M.P. Holland, D.A. Shaw, M.A. MacDonald, M.A. Hayes, L.G. Shpinkova, Chem. Phys. 236 (1998) 365.
[23] E.E. Rennie, C.A.F. Johnson, J.E. Parker, R. Ferguson, D.M.P. Holland, D.A. Shaw, Chem. Phys. 250 (1999) 217.
[24] E.E. Rennie, to be published.
[25] D.A. Shaw, D.M.P. Holland, M.A. MacDonald, M.A. Hayes, L.G. Shpinkova, E.E. Rennie, C.A.F. Johnson, J.E. Parker, W. von Niessen, Chem. Phys. 230 (1998) 97.
[26] S. Nagakura, M. Kojima, Y. Maruyama, J. Mol. Spectrosc. 13 (1964) 174.
[27] B. Vidal, J.N. Murrell, Chem. Phys. Lett. 31 (1975) 46.
[28] D.M.P. Holland, J.B. West, A.A. MacDowell, I.H. Munro, A.G. Beckett, Nucl. Instrum. Methods Phys. Res. B 44 (1989) 233.
[29] D.A. Shaw, D.M.P. Holland, M.A. MacDonald, A. Hopkirk, M.A. Hayes, S.M. McSweeney, Chem. Phys. 163 (1992) 387.
[30] S.G. Lias, J.F. Liebman, R.D. Levin, S.A. Kafafi, NIST Standard Reference Database 19A (1993).
[31] F.H. Field, J.L. Franklin, F.W. Lampe, J. Am. Chem. Soc. 79 (1957) 2665.
[32] J. Dannacher, Chem. Phys. 29 (1978) 339.
[33] T. Baer, G.D. Willett, D. Smith, J.S. Phillips, J. Chem. Phys. 70 (1979) 4076.
[34] D.P. Stevenson, Discuss. Faraday Soc. 10 (1951) 35.
[35] R.I. Hall, L. Avaldi, G. Dawber, A.G. McConkey, M.A. MacDonald, G.C. King, Chem. Phys. 187 (1994) 125.
[36] K. Codling, L.J. Frasinski, Contemp. Phys. 35 (1994) 243.
[37] NIST Chemistry Webbook. http://webbook.nist.gov
[38] H. Kuhlewind, A. Kiermeier, H.J. Neusser, J. Chem. Phys. 85 (1986) 4427.
[39] E.E. Rennie, C.A.F Johnson, J.E. Parker, D.M.P. Holland, D.A. Shaw, M.A. Hayes, Chem. Phys. 229 (1998) 107.
[40] M. Takezaki, N. Hirota, M. Terazima, H. Sato, T. Nakajima, S. Kato, J. Phys. Chem. A 101 (1997) 5190.
[41] A.D. Baker, D.P. May, D.W. Turner, J. Chem. Soc. B. (1968) 22.
[42] T. Kobayashi, S. Nagukura, Chem. Lett. (1972) 903.
[43] J.W. Rabalais, J. Chem. Phys. 57 (1972) 960.
[44] O.S. Khalil, J.L. Meeks, S.P. McGlynn, J. Am. Chem. Soc. 95 (1973) 5876.
[45] M.H. Palmer, W. Moyes, M. Spiers, J.N.A. Ridyard, J. Mol. Struct. 55 (1979) 243.
[46] K. Kimura, S. Katsumata, Y. Achiba, T. Yamazaki, S. Iwata, Handbook of HeI Photoelectron Spectra of Fundamental Organic Molecules, Japan Scientific Societies Press, Tokyo, 1981.
[47] S. Katsumata, H. Shiromaru, K. Mitani, S. Iwata, K. Kimura, Chem. Phys. 69 (1982) 423.
[48] L. Klasinc, B. Kovac, H. Güsten, Pure Appl. Chem. 55 (1983) 289.
[49] W.S. Chin, C.Y. Mok, H.H. Huang, S. Masuda, S. Kato, Y. Harada, J. Electron Spectrosc. Relat. Phenom. 60 (1992) 101.
[50] C.C. Turci, S.G. Urguhart, A.P. Hitchcock, Can. J. Chem. 74 (1996) 851.
[51] T. Ari, H. Güven, N. Ecevit, J. Electron Spectrosc. Relat. Phenom. 73 (1995) 13.
[52] M.R. Robin, Higher Excited States of Polyatomic Molecules, Vol II, Academic, New York, 1974.
[53] C. Sieiro, J.I. Fernandez-Alonso, Chem. Phys. Lett. 18 (1973) 557.
[54] O. Kröhl, K. Malsch, P. Swiderek, Phys. Chem. Chem. Phys. 2 (2000) 947.